Environmental Science & Technology

pubs.acs.org/est

Article

Modeling the Mercury Cycle in the Sea Ice Environment: A Buffer between the Polar Atmosphere and Ocean

Shaojian Huang, Feiyue Wang, Tengfei Yuan, Zhengcheng Song, Peipei Wu, and Yanxu Zhang*

Cite This: https://doi.org/10.1021/acs.est.3c05080

Read Online

ACCESS | Metrics & More | Article Recommendations | Supporting Information

ABSTRACT: Sea ice (including overlying snow) is a dynamic interface between the atmosphere and the ocean, influencing the mercury (Hg) cycling in polar oceans. However, a large-scale and process-based model for the Hg cycle in the sea ice environment is lacking, hampering our understanding of regional Hg budget and critical processes. Here, we develop a comprehensive model for the Hg cycle at the ocean−sea ice−atmosphere interface with constraints from observational polar cryospheric data. We find that seasonal patterns of average total Hg (THg) in snow are governed by snow thermodynamics and deposition, peaking in springtime (Arctic: 5.9 ng/L; Antarctic: 5.3 ng/L) and minimizing during ice formation (Arctic: 1.0 ng/L, Antarctic: 0.5 ng/L). Arctic and Antarctic sea ice exhibited THg concentration peaks in summer (0.25 ng/L) and spring (0.28 ng/L), respectively, governed by different snow Hg transmission pathways. Antarctic snow-ice formation facilitates Hg transfer to sea ice during spring, while in the Arctic, snow Hg is primarily moved through snowmelt. Overall, first-year sea ice acts as a buffer, receiving atmospheric Hg during ice growth and releasing it to the ocean in summer, influencing polar atmospheric and seawater Hg concentrations. Our model can assess climate change effects on polar Hg cycles and evaluate the Minamata Convention's effectiveness for Arctic populations.

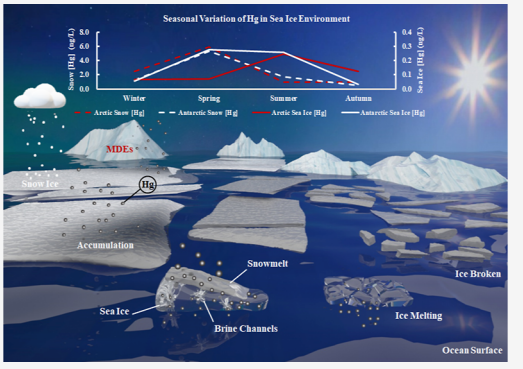

KEYWORDS: *mercury, sea ice, snow, polar oceans, MITgcm*

1. INTRODUCTION

The concentrations of mercury (Hg), a potent neurotoxin, in polar regions (the Arctic and Antarctic) have increased remarkably since the industrial revolution, which is often associated with the long-range transport of Hg from lower latitudes.[1−4] After being deposited in the polar marine environment, inorganic Hg can be converted to highly neurotoxic methylmercury (MeHg), which can be bioaccumulated and biomagnified in the food chain.[5−8] This has raised a great concern for indigenous people, especially in the pan-Arctic communities, because they rely on marine mammals and fish as part of their traditional diet.[1,9] A better understanding of Hg cycling in the polar regions is thus needed to better estimate the exposure risk of Hg and make effective mitigation and adaptation strategies.

A unique feature of the polar marine environment is the presence and dynamics of the sea ice environment (including the overlying snow), which is known to play a major role in the biogeochemical processes of Hg in the polar environment.[1,4,6,10−12] Sea ice is a reservoir of Hg with greater (~twofold) Hg mass per unit volume than surface seawater.[13] Recently, the Arctic sea ice environment has undergone a dramatic regime shift from predominantly multi-year ice (MYI) pack to one composed primarily of first-year ice (FYI),[14] indicating a potential change in the biogeochemical cycling of Hg in the Arctic system.[2] Hg dynamics, however, are more active within FYI than MYI due to the difference in the brine volume fraction.[2,8,15] The dynamic brine pockets and drainage channels in FYI promote permeability and facilitate the transport of gaseous and dissolved Hg.[15] In contrast, MYI undergoes severe desalination and crystal retexturing, leaving less brine pockets, and the Hg content in MYI is primarily determined by particle processes involving particulate matter that has been retained from sediment, snow, or other aerosol sources.[2] The overlying snow is especially effective in receiving Hg deposited from the atmosphere, especially during the springtime mercury depletion events (MDEs).[13,15] Although a considerable amount of the deposited Hg in snow can be re-emitted back to the atmosphere following rapid photoreduction,[16,17] some of the deposited Hg is retained in the snowpack[15] and enters the marine ecosystem upon the melting of the snowpack and ice.

Meteorological factors, especially sunlight and temperature, are primary drivers for the transport and transformation of Hg

Received: June 30, 2023
Revised: August 3, 2023
Accepted: August 4, 2023

across the ocean−sea ice−atmosphere (OSA) interface in the polar marine environment. In the cold seasons, continuous snowfall scavenges atmospheric Hg, which can be transformed into sea ice Hg through the formation of snow ice and via gas/brine migration. The Hg^0 in the snowpack can be transported via molecular and turbulent diffusions.[18] The former is slow but ubiquitous, while the latter is potentially faster but controlled by atmospheric turbulence, which is more variable and influenced by meteorological factors.[18−20] Most of the dissolved Hg species are rejected during the seawater freezing process, with the remainder enriched in the brine pocket of newly formed ice.[13,15] In warm seasons, snow melts, and the Hg in snow can be leached to the underlying ice surface. Rising temperature also alters the interior of newly formed ice, and Hg can be discharged from the sea ice to the underlying seawater along with the desalination process.[11,21,22] The exposure of supersaturated Hg^0 concentrations under contiguous ice also enhances evasion during sea ice melting.[23]

Our knowledge about the cycling of Hg in the polar marine cryosphere is improved by the accumulating field measurement.[2,15,23−27] New techniques such as stable Hg isotopes also begin to elucidate the redox chemistry of Hg in the polar marine cryosphere.[28−32] Nonetheless, large-scale process-based models are needed to describe the overall budget of Hg in the polar cryosphere, given the strong spatial and temporal heterogeneity of the polar environment.[17] Several studies have undertaken process-based atmospheric models to study the interaction between the atmosphere and the underlying snow surface or ocean.[33−35] However, these studies focused on the atmosphere or snowpack but neglected the sea ice, which is a key component of the polar cryosphere. In this study, we develop a new model for the Hg cycle in the polar sea ice and snow to integrate the field measurements and the understanding of Hg processes. The model is based on the sea ice module developed by Losch et al.[36] in the MIT General Circulation Model (MITgcm). Losch et al. demonstrated the application of a realistic, eddy-admitting, global ocean and sea ice configuration to showcase results from the Arctic and Antarctic regions.[36] They examined the performance of B-grid and C-grid dynamic solvers, along with other numerical details of the parameterized dynamics and thermodynamics, using a regional Arctic configuration. In addition, the original sea ice model components inherited from current-generation climate models were also reformulated on an Arakawa C-grid to align with the MITgcm oceanic grid, allowing it to better capture the intricate dynamics of the sea ice system within the model. This model is coupled with a global seawater Hg model within the same model framework developed by Zhang et al.[37,38] The model results are evaluated against available measurements. A budget of Hg is also calculated to further explore the role of snow and sea ice in the polar cryospheric Hg cycle.

2. METHODOLOGY

2.1. MITgcm. The global three-dimensional MITgcm is used to simulate the chemistry and transport of Hg in the ocean. Advection and diffusion of oceanic Hg are calculated based on the ocean state estimation from the Estimating the Circulation and Climate of the Ocean (ECCO v4) configuration.[39] The finite-volume discretization of the momentum equation is formulated on the Arakawa C-grid.[36] The model has a horizontal resolution of 1° × 1° and 50 uneven vertical layers ranging from 10 m near the surface to approximately 450 m at a maximum model depth of 6150 m. The resolution is higher over the polar regions (about 36 km × 36 km) to better represent the ocean currents.

2.2. Sea Ice Model. The MITgcm sea ice model is based on a variant of the viscous-plastic dynamic−thermodynamic sea ice model first introduced by Hibler.[40−42] Ice thermodynamics is represented by a zero-heat-capacity formulation. Heat, freshwater fluxes, and surface stresses are computed from the atmospheric state and modified by the ice model at every time step (1 h). The ice temperature is further calculated based on the net flux of heat and freshwater, and the changes in the ice thickness are determined. The parameterization of lateral and vertical growth of sea ice follows that of Hibler.[40,41] The dynamic and thermodynamic interactive sea ice model is tightly coupled to the ocean component of the MITgcm. The model uses the third-order direct space−time (DST) scheme for the horizontal advection.

The model performance is evaluated against the observed sea ice extents from the National Snow and Ice Data Center (NSIDC). We find that the model can capture the interannual and seasonal variability of sea ice extent (Figures S1−S3), indicating the reliability of the sea ice simulation in the model.[43] The sea ice model successfully reproduces both interannual and seasonal variations of the sea ice extent.[43] Moreover, the model generates ice concentration and thickness distributions that closely resemble observed values. Notably, the simulations demonstrate a significant correlation ($p < 0.01$) with observations in both March and September, as indicated by a correlation coefficient ranging from 0.83 to 0.95. In addition, the age of sea ice is also considered in the model (Figure S4). Sea ice that is less than 1 year old is assumed to be FYI, while sea ice that survives the summer melt is considered as MYI. The MITgcm model, although not able to fully reproduce the accurate sea ice age as compared to the data product from the NASA National Snow and Ice Data Center Distributed Active Archive Center (NSIDC DAAC), successfully captures the boundary between FYI and MYI (Figure S4). In addition, our model also shows that MYI is mainly located in the north of the Canadian Arctic Archipelago (CAA), which is also comparable with a previous study.[44]

Above the ice, there is a layer of snow also modifying the heat flux and the albedo as described in Zhang et al.[45] Precipitation data from 6-hourly ERA-Interim reanalysis fields are taken as the snow precipitation input. If enough snow is accumulated, its weight submerges the ice and the snow is flooded. The transformation of snow to ice is modeled by a simple mass conserving parameterization of snow ice formation (a flood-freeze algorithm following Archimedes' principle).[46] Snowmelt tendency is also calculated based on the atmospheric forcing and heat available from the ocean.

2.3. Atmospheric Hg Deposition. The Hg in sea ice and snow is mainly from the atmospheric dry and wet deposition, which is taken from the output of the GEOS-Chem model. The deposition flux is strongly associated with the bromine chemistry in polar regions, especially during the atmospheric MDEs.[47,48] The bromine chemistry over polar sea ice is calculated following Fisher et al.[34] In GEOS-Chem, atmospheric Hg^0 is oxidized by the bromine (Br) atom, with Br concentrations specified by the photochemical steady state. BrO concentrations in the boundary layer are a function of air temperature from Modern Era Retrospective-analysis for Research and Applications (MERRA). BrO_x radicals (BrO_x = Br + BrO) are assumed to generate in a polar 4° × 5° grid square in spring with adequate sea ice cover and incident shortwave radiation.[34] Both the re-

https://doi.org/10.1021/acs.est.3c05080
Environ. Sci. Technol. XXXX, XXX, XXX−XXX

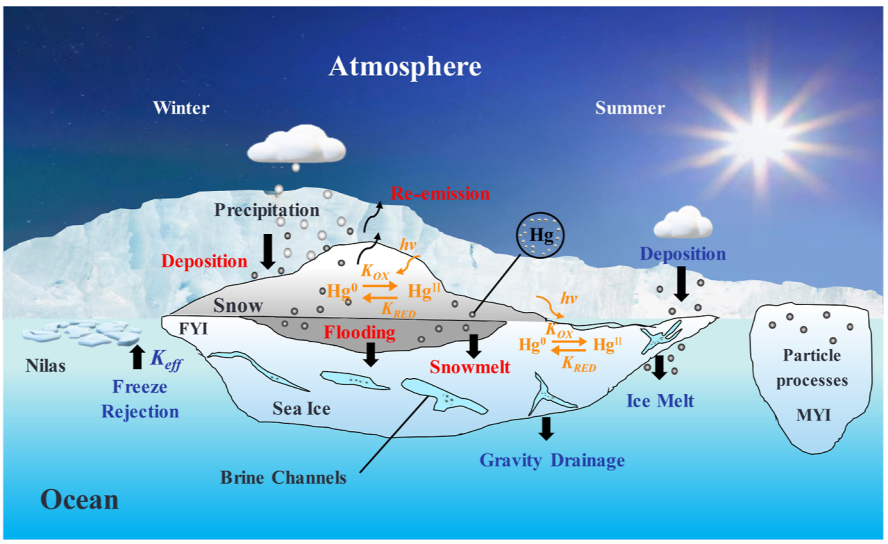

Figure 1. Schematics of Hg transport and transformation in the polar atmosphere−snow−sea ice−ocean environment (modified from Wang et al., 2017).[11] The red color represents the Hg migration in snow. The blue color stands for the behavior of sea ice Hg. The orange color represents the photochemical transformation of Hg in snow and sea ice. K_{eff} is the effective distribution coefficient of Hg during freeze rejection. K_{OX} and K_{RED} are the photo-oxidation and photoreduction rate coefficients of Hg, respectively, in snow and sea ice. FYI is short for first-year ice, and MYI is short for multi-year ice. This study only considers the Hg behavior in FYI.

emission and melting processes are also considered in the GEOS-Chem model. Specifically, the model assumes that 60% of the deposited Hg on the surface of snow and sea ice is rapidly re-emitted back into the atmosphere. Subsequently, the remaining 40% of the deposited particles are re-emitted during snow melting. The re-emissions from snow are parameterized based on solar radiation, using the effective rate constant estimated by Durnford and Dastoor.[17]

Different redox chemistry and emission inventories are considered in four GEOS-Chem model simulations for sensitivity analysis. The first one is based on the results from Horowitz et al.[49] with the global total emission from the WHET emission inventory for 2010.[50] Results from Song et al.[51] are taken as the second scenario, which is based on the scaled EDGARv4.tox2 inventory with other model setups following Horowitz et al.[49,51] In the third scenario, Hg emissions are also from WHET, while the atmospheric Hg redox mechanisms are updated by Shah et al.[52] For the last scenario, the chemical mechanism from Shah et al. and the scaled EDGAR v4.tox2 inventory are considered. To evaluate the impact of different atmospheric deposition schemes, we conduct a sensitivity test among four schemes (Figures S5 and S6). The sensitivity test reveals a similar monthly variation of snow Hg concentrations across all four schemes. Although the parameterization of atmospheric chemistry from Shah et al. results in higher spring atmospheric Hg deposition due to the improved OH-initiated oxidation of Hg^0 to Hg^{II},[52] there are no significant differences among the four schemes (p-values are 0.26 and 0.91 for the Arctic and Antarctic, respectively), indicating the robustness of our model with regard to the atmospheric input data.

2.4. Hg in Sea Ice. The transformation processes of Hg in sea ice and snow are illustrated in Figure 1. While our model includes sea ice of different ages, which influences the behavior of Hg, this study primarily focuses on the biogeochemical cycling of Hg in FYI due to the limited resolution of our model. Tracking the age of sea ice Hg and parameterizing the particle processes is not feasible with our current model. On the other hand, the decreasing trend in MYI coverage would ultimately lead to an ice-free summer Arctic, leaving only FYI.[53,54] We, thus, choose to neglect the particle processes in MYI and consider three pathways for Hg input to the FYI as suggested by Chaulk et al.:[15] (i) residual from seawater after freeze rejection, (ii) scavenged from the atmosphere at snow-free ice surfaces, and (iii) transported from the above snow cover. During sea ice formation, a fraction of dissolved Hg and particulate Hg can be trapped in the brine pockets, leading to their accumulation and enrichment within sea ice. The initial Hg content in newly formed sea ice is parameterized based on the initial ice salinity as suggested by Cox and Weeks.[22]

$$\mathrm{Hg_i} = K_{\mathrm{eff}} \times \mathrm{Hg_{sw}} \tag{1}$$

where $\mathrm{Hg_i}$ is the initial concentration of Hg in the bulk sea ice, $\mathrm{Hg_{sw}}$ is the concentration of Hg in seawater, and K_{eff} is the effective distribution coefficient

$$\begin{cases} K_{\mathrm{eff}} = \dfrac{0.26}{0.26 + 0.74\exp(-7243V)}, \\ \quad V > 3.6 \times 10^{-5} \\ K_{\mathrm{eff}} = 0.8925 + 0.0568 \ln V, \\ \quad 2.0 \times 10^{-6} < V < 3.6 \times 10^{-5} \\ K_{\mathrm{eff}} = 0.12, \qquad V < 2.0 \times 10^{-6} \end{cases} \tag{2}$$

where V is the ice growth velocity in cm/s.

The model considers two ways in which sea ice obtains Hg from the above snow cover: snow ice formation due to snow ice formation and snowmelt leaching. The thickness of snow ice is determined by snow precipitation. The snowmelt is modeled as a function of thermodynamic variables from the force field. Hg leaves sea ice mainly via ice melting, re-emission, and desalination. We assumed 67% of the Hg^0 deposited to the sea ice environment is re-emitted back to the atmosphere, based on studies on Hg^0 re-emission fractions from Arctic snowpack, which typically range from 40 to 90%.[17,26,27,55,56] A sensitivity test examining the impact of three re-emission fractions (77, 67, and 57%) reveals consistent seasonal patterns and minor

https://doi.org/10.1021/acs.est.3c05080
Environ. Sci. Technol. XXXX, XXX, XXX−XXX

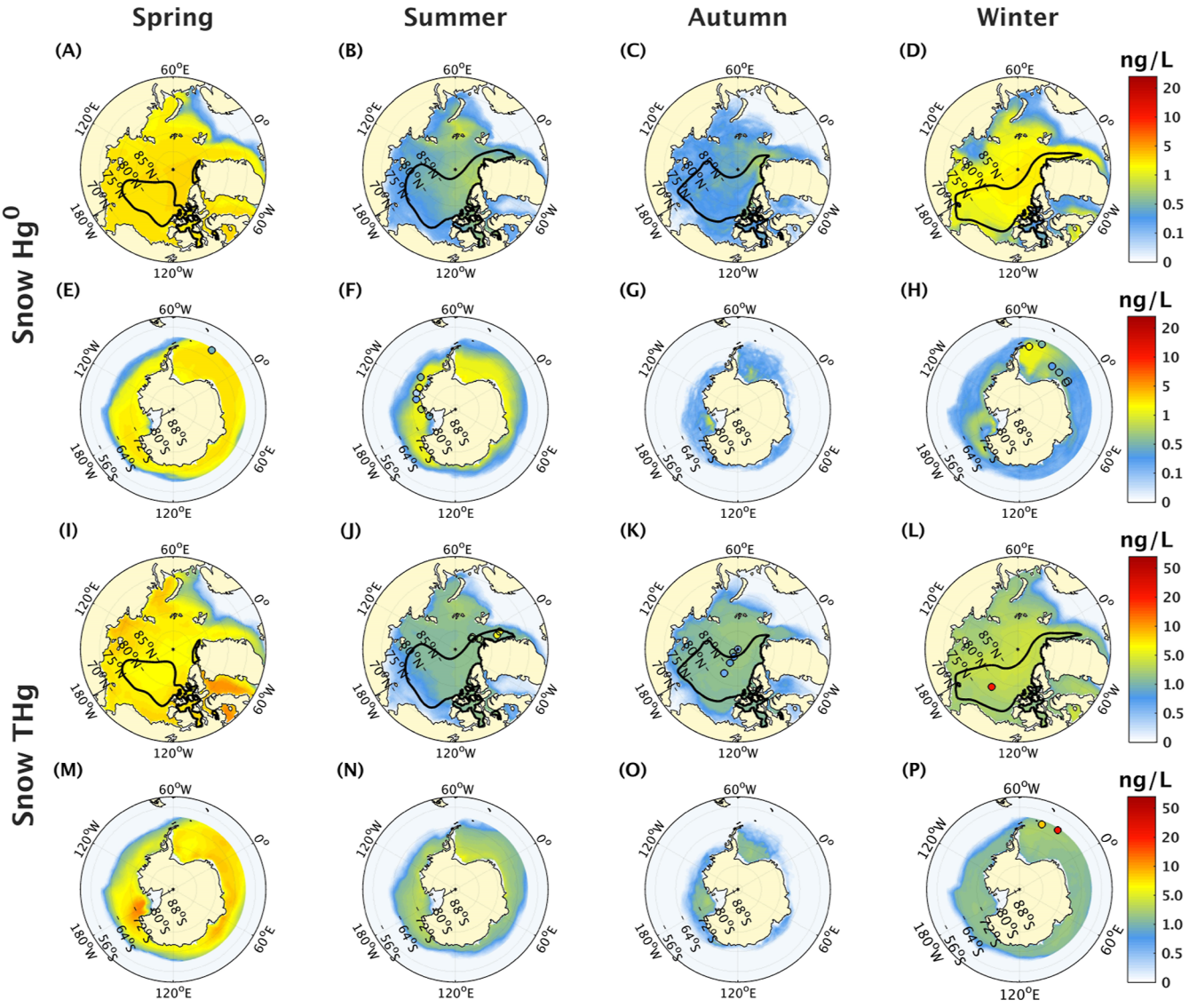

Figure 2. Seasonal average of Hg^0 (A to H) and THg (I to P) concentrations within snow in polar oceans. Summer refers to June−August (November−February), autumn refers to September−November (March−April), winter refers to December−February (May−August), and spring refers to March−May (September−October) in the Arctic (Antarctic). Observed concentrations of Hg^0 and THg in snow from previous studies are shown as circles.[13,23,71,72] Note the different color scales for Hg^0 and THg. The thick black contour marks the simulated boundary between FYI and MYI calculated from 2002 to 2011.

variations in summer Hg re-emission from ice (Figure S7). Salt in sea ice is dissolved within liquid inclusions of brine. The ice desalinates when this brine is progressively drained.[21,57] There are several pathways of desalination including brine expulsion, gravity drainage, and flushing.[58] Here, we only consider the gravity drainage process, which represents the influence of gravity on the interconnected brine network. The desalination rate is used as a proxy for the Hg releasing rate from sea ice interior

$$\frac{\partial S}{\partial t} = \delta(1 - \eta e)\frac{\partial T}{\partial z} \quad (3)$$

where S is the salinity of sea ice and δ and η are empirical coefficients. δ is set to 5.88×10^{-8} $°C^{-1}·m·s^{-1}$, and η equals 20 according to Vancoppenolle et al.[58] e is the relative volume of brine inclusions. $\frac{\partial T}{\partial z}$ is the temperature gradient of sea ice. Due to the limitation of models in representing different sea ice layers, we approximate the temperature gradient by using the ratio of temperature difference before and after ice growth, along with the ice thickness.

2.5. Hg in Snow. The input of snow Hg mainly originates from atmospheric deposition. The snowfall can accelerate the scavenging of atmospheric Hg including the gaseous form Hg^{II} and those absorbed by particles.[59,60] The Hg concentrations of newly precipitated snow are calculated based on the wet deposition of Hg from GEOS-Chem and snow depth. Hg in snow would transport to sea ice via either snowmelt or snow flooding depending on the thermal variation of snow within the snowpack model. Normally, snowmelt supplies freshwater to form melt ponds.[61] When the snow melts, all the Hg in snow melting water is assumed to enter the sea ice.

We consider the molecular diffusion transport of Hg^0 in our model. The fractions of Hg^0 re-emission from snow on sea ice are lower than those on coastal land because the elevated chloride levels derived from marine sources can suppress the Hg^{II} photoreduction.[62] Hence, the re-emission processes only

https://doi.org/10.1021/acs.est.3c05080
Environ. Sci. Technol. XXXX, XXX, XXX−XXX

involve the newly deposited Hg on the active snow layer of 30 cm. An *e*-folding depth (i.e., the depth where the intensity of solar radiation decreases by a factor of *e*) of 7.5 cm is also set for incident shortwave radiation following Durnford et al.[56] The transfer of Hg from the snow surface to the atmosphere is calculated based on Durnford et al.[56]

$$\mathrm{Emi}_{\mathrm{Gtop}} = K_{\mathrm{topA}} \times (G_{\mathrm{top}} - G_{\mathrm{atm}}) \tag{4}$$

where $\mathrm{Emi}_{\mathrm{Gtop}}$ is the emission of Hg^0 from the active layer to the atmosphere, K_{topA} is the transfer coefficient from the top snow layer, and G_{top} and G_{atm} are the concentrations of Hg^0 in the active layer and the atmosphere, respectively.

$$K_{\mathrm{topA}} = \frac{D_{\mathrm{mol}}}{L} \tag{5}$$

where D_{mol} is the effective rate of molecular diffusion of Hg^0 within the snow and the value of D_{mol} is set to 6.0×10^{-6} m^2 s^{-1}, and L is the characteristic path length valued at $H_{\mathrm{snow}}/2$, with H_{snow} being the height of the active snow layer.

$$D_{\mathrm{mol}} = \frac{\phi}{\tau} \times D_{(T,P)}^{\mathrm{surface}} \tag{6}$$

$$D_{(T,P)}^{\mathrm{surface}} = D_{T_0,P_0} \times \frac{P_0}{p} \times \left(\frac{T}{T_0}\right)^{1.85} \tag{7}$$

where $D_{(T,P)}^{\mathrm{surface}}$ is the Hg^0 diffusivity in the atmosphere.,[63,64] D_{T_0,P_0} is the coefficient of diffusivity at standard temperature and pressure (STP) with the value being set to 0.1243,[64] ϕ is the snow porosity with the value being set to 0.637, and τ is the firn tortuosity with the value being set to 2.0.[63]

The model includes the photochemistry of Hg in the snow and sea ice. The photo-oxidation (K_{OX}, s^{-1}) and photoreduction (K_{RED}, s^{-1}) rate coefficients are calculated based on radiation intensity (R, W m^{-2}).[30]

$$K_{\mathrm{OX}} = 4.32 \times 10^{-6} \times R \tag{8}$$

$$K_{\mathrm{RED}} = 8.35 \times 10^{-6} \times R \tag{9}$$

2.6. Hg in Seawater. The simulation of inorganic Hg species in seawater is based on the MITgcm-Hg model built by Zhang et al.[37] Aqueous Hg species (Hg^0 and Hg^{II}) undergo photo-biological-mediated transformation following Soerensen et al.[65] The dissolved Hg^{II}, adsorbed to suspended matters, can form particulate-bound mercury (Hg^P), and the absorbed fraction is calculated based on a constant partition coefficient and local particulate organic carbon (POC) concentrations. Hg^P sinks to the deeper ocean by POC scavenging. The marine biogeochemical and ecological parameters (e.g., POC concentrations and sinking fluxes) are from the Darwin model.[66] More details about the configuration of the ocean model can be found in Zhang et al.[38]

2.7. Observation Data Sets. To evaluate our model, the observed Hg concentrations in sea ice environments were obtained from multiple expeditions in the Arctic and Southern Oceans, as shown in Table S1. For instance, ice core samples collected by Chaulk et al. in the southern Beaufort Sea of the Arctic from March to September 2005 provided valuable data on Hg concentrations in sea ice.[15] Surface snow THg concentrations from the GEOTRACES Arctic Ocean cruise in 2015 were included as another data set for evaluation.[23] Hg^0 concentrations in the sea ice environment were derived from Nerentorp Mastromonaco et al. (sampling conducted from December 2010 to January 2011 and August to October 2013).[13] The observation data also include some limited ice cores collected from MYI regions.[2,15] Given the limited availability of such data, we used the average Hg concentrations across the entire MYI core as a representative measure of Hg content in FYI.

2.8. Models Running. The atmospheric forcing data that serve as the upper boundary layer of the ocean (e.g., near-surface wind speed, air temperature, short-wave and long-wave radiations) are from the ERA-interim reanalysis, a climate reanalysis dataset, spanning 1992−2017.[67] The input of Hg from river freshwater runoff to coastal oceans is from Liu et al.[68] To ensure computational efficiency, we run the model for 20 years from 1992 to 2011 with a time step of 3600 s. The initial 10 years served as a spin-up period, allowing the surface ocean (0−50 m)[66] and sea ice components to reach a steady state. This critical step ensured the accuracy and reliability of our analysis. To establish a solid foundation for our conclusions, we exclusively considered the average results obtained during the final 10 years of the simulation.

3. RESULTS AND DISCUSSION

3.1. Snow Hg. The modeled snow Hg concentrations exhibit clear seasonal variation (Figure 2). In general, snow Hg concentrations increase from winter and peak in spring for both the Arctic Ocean and the Southern Ocean (hereafter, we refer to their local seasons, i.e., boreal and austral for the north and south hemispheres, respectively) due to the enhanced Hg deposition (Figure S8). In the Arctic spring, the spatial pattern of snow Hg^0 concentrations reflects the atmospheric deposition and the re-emission of Hg^0. The simulated deposition flux of THg is predominant along the Arctic coastal region. Our results show a similar spatial distribution of Hg^0 re-emission as observed for THg deposition, suggesting a net production of Hg^0 through photoreduction processes in the Arctic coastal region, attributed to higher levels of shortwave radiation.[69,70] Furthermore, our findings indicate an intense re-emission of Hg^0 in the Arctic coast region, resulting in lower concentrations of Hg^0 in the snow within the FYI area. Overall, the modeled snow Hg^0 concentrations are 2.3 ± 0.6 ng/L during the Arctic spring. Hg^0 re-emissions from snow are higher in lower latitude regions corresponding to the intensive photoreduction of oxidized Hg (Figure S9). Most of the snow starts to melt with the rising temperature in summer, and snow Hg^0 concentrations decrease to 0.37 ± 0.11 ng/L and even lower in autumn (0.24 ± 0.07 ng/L). The modeled THg concentrations exhibit a seasonal pattern that closely resembles that of Hg^0 concentrations. Specifically, snow THg concentrations show a substantial increase of more than twofold from the dark winter (2.3 ± 0.70 ng/L) to the sunlit spring period (5.9 ± 1.6 ng/L). This observed increase is consistent with a previous study, which reported a similar fourfold rise in snow Hg concentrations from winter to spring.[71]

In the Southern Ocean, the modeled snow THg concentrations have a similar seasonal variation to the Arctic, peaking in spring (5.3 ± 1.7 ng/L) and dropping to the minimum in autumn (0.52 ± 0.20 ng/L). However, during winter, the snow TH concentrations in the Southern Ocean (1.3 ± 0.42 ng/L) are only half of those modeled in the Arctic Ocean (2.5 ± 0.7 ng/L). Interestingly, in summer, the snow TH concentrations show a different pattern, with the Southern Ocean (1.70 ± 0.60 ng/L) exhibiting nearly 50% higher levels compared to the Arctic Ocean (0.95 ± 0.27 ng/L). This seasonal difference can be

https://doi.org/10.1021/acs.est.3c05080
Environ. Sci. Technol. XXXX, XXX, XXX−XXX

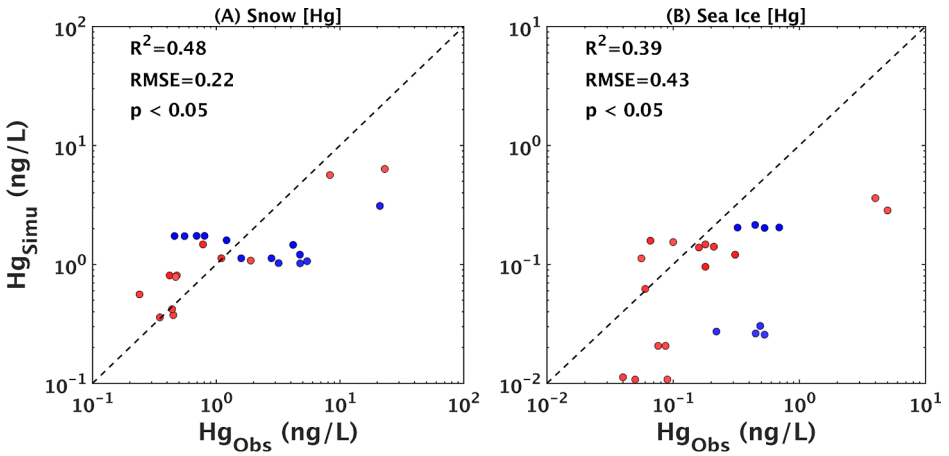

Figure 3. Comparison of simulated Hg concentrations (ng/L) in the snow (A) and sea ice (B) with observations. RMSE is the root-mean-square error with the base-10 logarithm-transformed values. R^2 is the coefficient of determination. Both R^2 and RMSE are calculated based on the difference between modeled and observed concentrations. The blue and red colors represent the Arctic Ocean and the Southern Ocean, respectively.

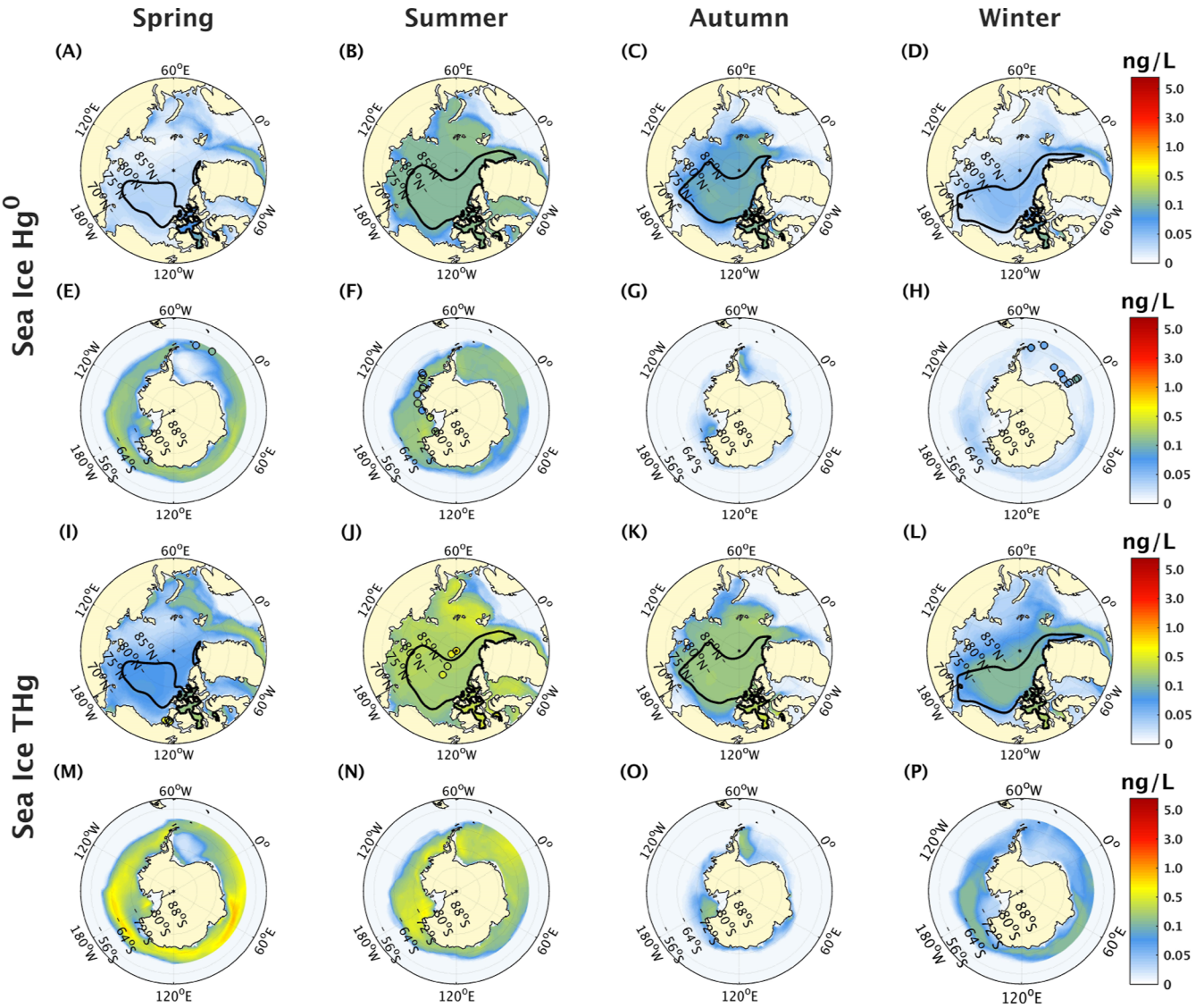

Figure 4. Seasonal average of Hg^0 (A–H) and THg (I–P) concentrations within sea ice in polar oceans. Summer refers to June–August (November–February), autumn refers to September–November (March–April), winter refers to December–February (May–August), and spring refers to March–May (September–October) at the Arctic (Antarctic). Observed concentrations of Hg^0 and THg in sea ice from previous studies are shown as circles.[2,4,13,15] The thick black contour marks the simulated boundary between FYI and MYI calculated from 2002 to 2011.

https://doi.org/10.1021/acs.est.3c05080
Environ. Sci. Technol. XXXX, XXX, XXX−XXX

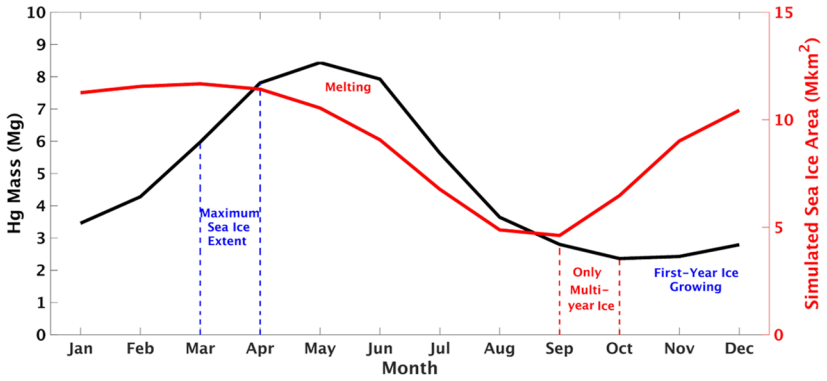

Figure 5. Monthly variation of Hg mass in Arctic sea ice environments (including sea ice and the above snow layer). The maximum sea ice extent occurs in March. All the FYI melts away in September, with only MYI left behind. The red line represents the simulated monthly sea ice area (Mkm^2) variation.

explained by the difference between the sea ice and snow environments in the Arctic and the Southern Ocean. The Antarctic sea ice extent is substantially smaller than its counterpart around the Arctic right after the melting season, leaving less place for snow cover.[73] From winter to spring, prominent deposition induced by heavier snowfall surges the Hg concentrations in Antarctic snow, reducing the hemispheric differences in snow Hg concentrations. Such clear seasonal variation of snow Hg would inevitably affect the snow-involved transmission of Hg and hence alter the Hg distribution between the overlying atmosphere and underlying sea ice.

Observational data for the Hg distribution in the polar cryosphere remain sparse. Figure 3 shows a comparison between simulated Hg concentrations and observations in sea ice environments. The data points cluster around the 1:1 line with a statistically significant correlation relationship ($p < 0.05$). The root-mean-square errors (RMSEs) are 0.22 and 0.43 for the snow and sea ice Hg concentrations, respectively, with coefficients of determination (R^2) of 0.48 and 0.39, indicating a reasonable agreement between the model and observations. The model-observation discrepancy mainly occurs in snow THg concentrations in autumn and winter, especially for the Southern Ocean. For instance, measurement data show that winter snow THg concentration in the northern Weddell Sea is 39 ng/L, larger than that in the Arctic Ocean (21 ng/L).[13,71] Thicker snow cover was observed in the Weddell Sea area with second-year ice.[74] The higher THg concentrations could thus be attributed to the longer accumulation period in the Antarctic.

Our model probably underestimates the atmospheric Hg deposition in the Antarctic during winter because the model only considers the BrOx generation in the springtime, which favors the oxidation of Hg^0 and leads to higher Hg^{II} deposition flux.[34] Besides, unique physical and chemical processes in the cryosphere can also enrich Hg concentrations in polar snow that consists of multiple distinct layers.[17,75] However, our model only contains a single snow layer with zero heat capacity. The seasonal variability of the thickness of the snow could be exaggerated, leading to an underestimation of the long-term accumulation of Hg.

3.2. Sea Ice Hg. Figure 4 shows a distinct seasonal variation of modeled Hg concentrations in sea ice in the Arctic Ocean and the Antarctic Ocean. The modeled Arctic sea ice THg concentrations peak in summer (0.25 ± 0.07 ng/L) right after the spring maximum of snow Hg, while the highest THg concentrations in Antarctic sea ice occur in spring (0.26 ± 0.09 ng/L). The lowest value of sea ice THg is modeled in winter (0.07 ± 0.02 ng/L) in the Arctic and in autumn (0.03 ± 0.02 ng/L) in the Antarctic. The hemispheric difference in the seasonal transmission of snow Hg primarily drives such a pattern. Arctic sea ice Hg concentrations maximize in summer mainly due to the loss of melting snow cover. The melting snow would, on the one hand, transfer the snow Hg to the underlying sea ice and would, on the other hand, uncover the sea ice allowing atmospheric Hg to deposit directly on snow-free sea ice. The spring maximum of Hg concentrations in Antarctic sea ice is, nevertheless, associated with the more pronounced snow-ice formation from snow flooding. Oxygen isotope signature ($\delta^{18}O$) showed considerable proportions (8−38%) of snow ice in Antarctic ice cores, while the formation of snow ice was relatively uncommon in the Arctic.[76,77] The snowpack becomes saltier as brine is wicked up, carrying more Hg than the sea ice below. Therefore, the formation of snow ice greatly increases the Hg concentrations in Antarctic sea ice. Later, the Hg concentrations in polar sea ice start to decrease as the ice melts, releasing sea ice Hg into the ocean.

Sea ice covers start to expand in autumn when the temperature is dropping. Nevertheless, the impact of sea ice expansion on the THg concentrations of sea ice is also different between the Arctic Ocean and the Southern Ocean. In the Arctic Ocean, sea ice THg concentrations decline from autumn (0.13 ± 0.04 ng/L) to winter along with pronounced ice growth. Freeze rejection happens as sea ice volume increases, which dilutes the Hg concentrations in sea ice and results in the lowest value of Hg in winter. Nevertheless, the sea ice THg concentrations in the Antarctic are elevated from autumn to winter (0.06 ± 0.02 ng/L) along with sea ice formation. The Antarctic sea ice thickens from autumn to winter corresponding to the increasing snow accumulation[78] and, accordingly, the enhanced snow-ice formation elevates the Hg concentrations in Antarctic sea ice by transmitting Hg from Hg-enriched snow to sea ice.

Our model captures the seasonal variation of sea ice Hg as the observation. The concentrations of Hg^0 in Antarctic ice cores in three seasons (winter, spring, and summer) were analyzed by Nerentorp Mastromonaco et al.[13] with the values increasing from 0.07 to 0.12 ng/L. This increasing pattern in the Hg^0 concentrations is also simulated by our model from winter (0.013 ± 0.005 ng/L) to summer (0.11 ± 0.04 ng/L) (Figure 4E−H). However, the simulated THg concentrations of the southern Beaufort Sea during the summer season exhibit an underestimation, possibly attributed to the atmospheric MDEs. Chaulk et al.[15] measured the THg concentrations of the Arctic

https://doi.org/10.1021/acs.est.3c05080
Environ. Sci. Technol. XXXX, XXX, XXX−XXX

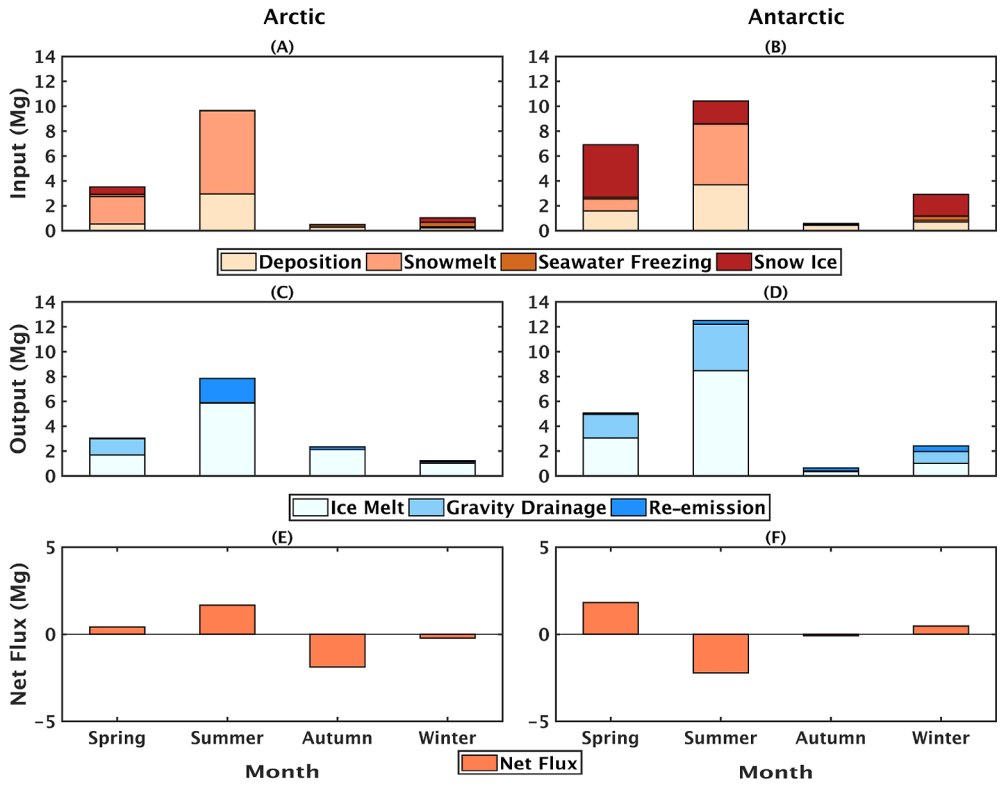

Figure 6. Seasonal THg fluxes of various processes to the sea ice. A, C, and E are for the Arctic, while B, D, and F are for the Antarctic. A and B represent the input THg flux to sea ice including deposition, snowmelt, seawater freezing, and snow ice. C and D show the output THg flux from sea ice via ice melt and gravity drainage. E and F show the net THg flux to sea ice.

newly formed ice in four stations, and the values ranged from 0.22 to 0.53 ng/L. Higher Hg concentrations (0.45−0.53 ng/L) were spotted in three stations undergoing MDEs, while the Hg concentration was 0.22 ng/L in the station with no occurrence of MDEs. However, our model is unable to capture the spring peak of sea ice Hg due to the incomplete MDE process in the current GEOS-Chem model. This could decrease the Hg input from the atmosphere to the sea ice, causing lower simulated Hg concentrations in sea ice.

3.3. FYI and MYI in the Arctic Ocean. The mass of Hg in the Arctic sea ice environments (including the above snow cover) is strongly influenced by the ice content and the age and thickness of the snow cover. Newly formed sea ice tends to carry more Hg than older ice. As illustrated in Figure 5, the total mass of Hg in Arctic sea ice increases from 2.4 to 8.4 Mg with the expansion of the sea ice area. As FYI grows, the boundary between FYI and MYI shows a rapid increase in Hg concentrations in FYI (Figure 2IL) due to enhanced deposition induced by snow precipitation (Figure S8), while Hg concentrations in MYI decrease (Figure 4I,L). Abundant brine pockets and channels in FYI retain the Hg from freeze rejection and atmospheric deposition in new ice, causing a net increase in Hg mass. The Hg content is continuously enriched after the sea ice extent reaches its maximum, and the Hg mass in sea ice starts to diminish due to the melt process. About 60% of the enriched Hg is removed from FYI via ice melting during the summer. The Hg mass of Arctic sea ice reaches its minimum after September when nearly all the FYI melts away, only leaving MYI that has survived through the melt seasons. This result also indicates a higher Hg mass in FYI than that in MYI, consistent with observations.[2] However, our model cannot track the age of sea ice Hg or differentiate the Hg behavior between FYI and MYI (Figure S4). We thus focus on the total Hg transport in the sea ice environments. As previously mentioned, the Hg processes have the same influence on both Hg concentrations and mass in sea ice. However, their seasonal patterns differ due to the distinct thermodynamic properties of snow and ice.

3.4. Fluxes of Key Processes. Seasonal waxes and wanes of sea ice determine Hg concentrations by greatly impacting the transport and transformation of Hg. Figure 6 (Figure S10) provides insights into the Hg fluxes within sea ice (snow) across different seasons. During Arctic spring, MDEs contribute (∼4 Mg) to Hg input in the snow cover, resulting in a doubling of springtime snow THg concentrations compared to winter levels. As summer arrives, the rising temperatures trigger the transfer of Hg (∼6.7 Mg) from snow to sea ice through snowmelt. This pathway accounts for approximately 70% of the total Hg input in sea ice, causing a more than twofold increase in sea ice THg concentrations and a reduction of over 80% in snow THg concentrations. Additionally, the snow-free sea ice accumulates deposited Hg (∼3 Mg) from the atmosphere, contributing to the major input of sea ice Hg mass in mid-late summer. Concurrently, a fraction of deposited Hg (∼2 Mg) is re-emitted back into the atmosphere from the snow-free sea ice surface. Despite a substantial release of Hg (∼5.9 Mg) into the ocean during ice thawing, the larger input of Hg from snowmelt and atmospheric deposition leads to a net Hg input into the sea ice. As the ice season commences, ongoing sea ice melting results in a net release of Hg (∼1.9 Mg) from the ice to the ocean. However, the overall Hg mass in the sea ice environments gradually accumulates (Figure 5) alongside sea ice growth and snowfall. The accumulated snowfall contributes to increased THg concentrations in snow, while the general sea ice THg concentrations experience a slight reduction due to the rapid

https://doi.org/10.1021/acs.est.3c05080
Environ. Sci. Technol. XXXX, XXX, XXX−XXX

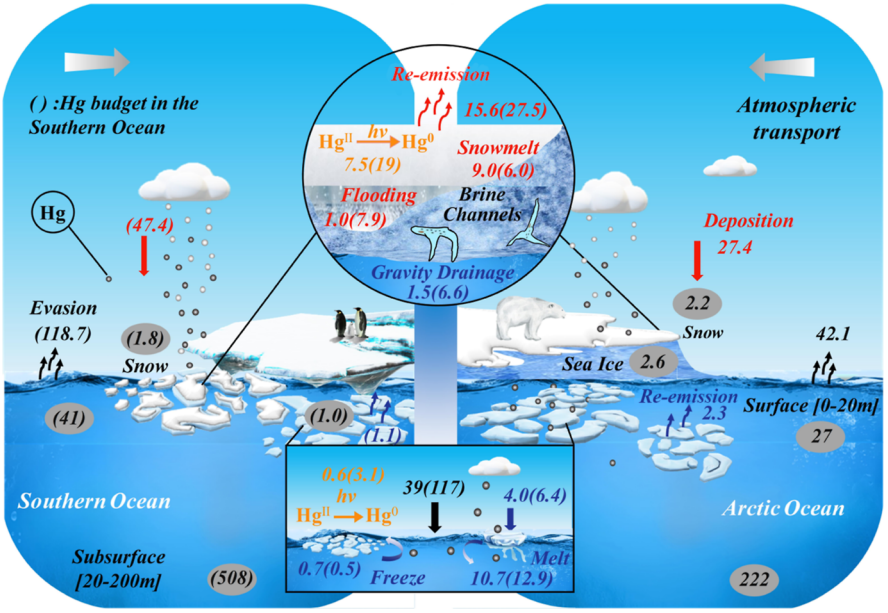

Figure 7. Mercury (Hg) cycle in the Arctic Ocean (>60°N) and the Southern Ocean (>60°S). The Hg cycle includes the atmosphere−snow-ice−ocean inter-compartmental fluxes (Mg/a). Red color stands for the Hg migration in snow. Blue color represents the behavior of Hg in sea ice. Black arrows show the Hg fluxes on the ocean surface. Orange color stands for the photo-redox of Hg in snow or sea ice. The estimates of the Hg mass reservoir in sea ice, snow, and surface water are shown in the gray oval (Mg). The zoomed circle and rectangle show the detailed transformation fluxes in the snow and sea ice, respectively. The numbers inside are for the Arctic, and those in parentheses are for the Antarctic.

expansion of sea ice volume, indicating an inverse relationship between the growing sea ice environments and THg concentrations during the ice season.

Although the Hg flux patterns in the Antarctic sea ice environments exhibit similarities to those in the Arctic, the role of snow is more vital in the Antarctic context. Notably, the observed THg concentrations in Antarctic sea ice (4.7 ng/L) are considerably higher than those in Arctic sea ice (0.42 ng/L) during spring,[13,15] despite the Antarctic being less influenced by anthropogenic factors. This disparity is primarily attributed to heavier snowfall and frequent snow flooding (i.e., the formation of snow ice), which facilitate greater atmospheric deposition and contribute to elevated THg concentrations in Antarctic sea ice.[77] The Antarctic snowpack accumulates substantial amounts of Hg starting from late winter, driven by the high reactivity of Hg^0 and occurrence of Hg^{II} deposition.[25] Our model reveals that snow flooding accounts for 37.8% of the Hg input to Antarctic sea ice while representing only 6.8% of the Hg input to Arctic sea ice. Through the process of snow-ice formation, the Hg-enriched snowpack leads to a more than fourfold increase in Antarctic sea ice THg concentrations. Additionally, the hemispheric disparity in the net flux of sea ice Hg during the melting season can be attributed to the presence of MYI. Unlike the Arctic, the release of Hg from Antarctic sea ice is greater and more facile due to the absence of MYI, which otherwise retains particle-bound Hg and inhibits its release.[2] By integrating the seasonal Hg transport fluxes within the sea ice environment, we can construct a more comprehensive Hg budget that captures the intricate dynamics of Hg cycling.

3.5. Mercury Budget in Polar Sea Ice. Figure 7 illustrates the annual budget of Hg in the polar sea ice. The sea ice environment serves as a net source to both the Arctic Ocean and the Southern Ocean. The unique wax and wane of this environment facilitate the seasonal transport of Hg, which distinguishes the polar marine Hg cycle from that observed in ice-free open oceans. Within this environment, snow plays a pivotal role in the transmission of Hg between the atmosphere and sea ice. In the Arctic Ocean, snow receives most of the atmospheric Hg from the deposition (27.4 Mg/a). The deposited Hg on shallow snow undergoes a photochemical transformation. Our model suggests a net photoreduction of 7.5 Mg/a Hg^0 from Hg^{II} in the snowpack, and 15.6 Mg/a of Hg^0 is re-emitted back to the atmosphere through molecular diffusion. Snowmelt is another pathway to transfer the snow Hg^{II} to sea ice with a flux of 9.0 Mg/a. The overall residence time of snow Hg is about 0.94 months. This means that most of the snow Hg obtained from atmospheric deposition is rapidly transferred to the atmosphere through re-emission or to the underlying sea ice via snowmelt. Indeed, the Arctic sea ice is almost snow-free during August, and snow begins to reaccumulate in September.[79] The short residence time and the low snow load lead to a small Hg pool in the snow (2.2 Mg).

Sea ice plays a bigger role than snow does on the Hg exchange at the air−sea interface. After the snow atop melts away, sea ice is directly exposed to atmospheric deposition of Hg. Apart from snowmelt, the largest input of sea ice Hg is from the atmospheric deposition (~4.0 Mg/a), followed by snow flooding (~1.0 Mg/a) and seawater freezing (~0.7 Mg/a). The low input from seawater freezing is because most of the dissolved substances (including Hg^{II}) are expelled during sea ice formation.[80] However, the Hg from the atmosphere can be only temporarily retained in the sea ice environments, with 24% flowing into the seawater through gravity drainage and ice melting from winter to spring. Furthermore, the rising temperature in the following summer eventually breaks the fragile storage by thawing the sea ice. About 10.7 Mg/a of Hg leaves sea ice via melting, taking up 74% of the total output. Sea ice is, thus, an important Hg source of surface seawater. The overall residence time of Hg in the Arctic sea ice is about 1.8 months, approximately twofold longer than that of snow Hg. In our study, the calculated residence time of Hg represents the overall situation in sea ice environments, which mainly consisted of FYI in both polar regions. This may

https://doi.org/10.1021/acs.est.3c05080
Environ. Sci. Technol. XXXX, XXX, XXX−XXX

potentially underestimate the residence time of Hg in the MYI because the model did not include Hg processes specific to MYI, which is mainly in particle-bound form and less prone to brine movement.[15] The size of the Arctic sea ice Hg reservoir in this study ranges from 1.5 to 5.7 Mg throughout the year with an annual average of 2.6 Mg.

The results of our model generally agree with those of previous studies (e.g., Dastoor et al.[3]) with similar Hg pool sizes. Our model simulates an evasion flux of Hg^0 of 42.1 Mg/a from the Arctic Ocean, which is also consistent with that reported by Dastoor et al.[3] (range 23−45 Mg/a). The total atmospheric deposition flux of Hg to the Arctic Ocean (70.4 Mg/a) observed in our model is similar to that of Dastoor et al.[3] (64.5 Mg/a). In addition, we further calculate the deposition of Hg to both the sea ice environment and the open ocean in the Arctic Ocean. Our model shows only 39 Mg/a deposition to the open ocean, with 27.4 and 4.0 Mg/a deposition to the snow and sea ice, respectively (Figure 7). This different input pathway of Hg may have important implications for the seasonal cycle of Hg^0 evasions and atmospheric Hg concentrations. Overall, our model simulates a 17.9 Mg/a re-emission flux of Hg^0 from Arctic sea ice and snow, and hence, the Arctic sea ice environment is a net sink of Hg (10.6 Mg/a) for the atmosphere.

The Hg budget in the Southern Ocean is generally similar to its Arctic counterpart. One difference is a larger fraction (37.8%) of sea ice Hg from snow flooding (7.9 Mg/a), which is nearly 10-fold higher than that of the Arctic sea ice. The annual average Hg concentrations in Antarctic sea ice are, therefore, roughly 23% higher than that in Arctic sea ice. In addition to, as we mentioned before, the ubiquitous snow ice formation in the Antarctic, a larger deposition rate of Hg (~47.4 Mg/a) provides more snow Hg input owing to higher Hg^{II} particle fraction at a lower temperature.[52] The net production of Hg^0 from Hg^{II} in snow via photo reaction is, accordingly, also twofold higher (19.0 Mg/a) than its counterpart around the Arctic and thus results in 27.5 Mg/a of Hg^0 re-emitting back to the atmosphere. The thick snow covering in the Antarctic sea ice is more capable of resisting melting than the Arctic due to the roughly one-magnitude-lower thermal conductivity than that of sea ice.[81] Thus, only 6.0 Mg/a of Hg in the Antarctic snowpack transfers to the underlying sea ice via snowmelt. Besides, atmospheric deposition provides 6.4 Mg/a of Hg to the snow-free ice surface. Nevertheless, most Antarctic sea ice, unlike Arctic sea ice, melts during summer and releases about 12.9 Mg/a of Hg to the Southern Ocean. The rapid wax and wane of Antarctic sea ice results in even smaller reservoirs of Hg (1.0 and 1.8 Mg in Antarctic sea ice and snow, respectively) as well as shorter residence times of Hg (0.6 and 0.9 months for snow Hg and sea ice Hg, respectively). The sea ice environment in the Southern Ocean also acts as a sink of atmospheric Hg with a net input (23.9 Mg/a) to the ocean surface from the atmosphere (Figure 7).

3.6. Uncertainty and Implications. Our model is subject to two primary uncertainties. First, the simple dynamics applied in the sea ice models does not consider variable heat capacity in the ice layer, resulting in a zero heat capacity that limits the storage of heat and thus amplifies the seasonal variability in the ice thickness. The upward conductive heat flux is parameterized based on a linear temperature profile and a constant ice conductivity. The conductive heat flux depends strongly on the ice thickness and atmospheric/oceanic thermal forcing. This could magnify the response of sea ice seasonal variability, although it does not change its overall pattern.[36] Second, a lack of detailed representation of MYI in our model constitutes an additional source of uncertainty as particulate Hg from the air and melt ponds can be significantly enriched in the surface of MYI.[11] The retention of particle-bound Hg in the topmost layer of MYI, where there is very little brine movement, contributes to the underestimation of sea ice Hg in our model.[2] Furthermore, particle entrapment, such as that promoted by rising ice crystals in newly forming ice,[82,83] also contributes to the uncertainty in our results. The parameterization scheme for this mechanism is limited, highlighting the need for further investigation. In addition, there is some discrepancy between the GEOS-Chem snow/ice Hg module and the MITgcm-Hg model, but it would be a second-order term for the snow/ice Hg budget itself. We will evaluate it by dynamically coupling these two models in our future research.

Our study provides a more accurate assessment of the polar ocean Hg budget, particularly for the Arctic, where the Hg cycle is under debate,[3,34,84] by incorporating detailed transport and transformation processes of Hg in snow and sea ice in our model. Despite their relatively small storage capacity, snow and sea ice play a crucial role in moderating the Hg cycle between the atmosphere and the ocean in the polar regions. Snow cover serves as a temporary sink for the atmospheric Hg and a source of Hg to sea ice, with a majority of deposited Hg^{II} gradually transferred to the underlying sea ice via snowmelt. Sea ice also effectively slows down the migration of Hg from the atmosphere to the ocean by retaining Hg in the semi-enclosed brine channel system inside. With rising temperatures, the retained Hg in sea ice becomes a source of Hg to the surface ocean. Thus, snow and sea ice in polar oceans function as a buffer between the atmosphere and the ocean, retaining the net atmospheric Hg input during cold seasons and releasing it during warmer seasons, which has implications for air−sea exchange of Hg^0 along with the variation of sea ice cover and Hg concentrations in the surface ocean. Overall, our model provides a useful framework for understanding the behavior of Hg in the polar cryosphere, especially for the Arctic Ocean, which is rapidly transitioning to an FYI regime with a greater capability of carrying Hg, potentially affecting the biota in sea ice habitats. The anticipated ice-free conditions in the Arctic Ocean during summer by the mid-2050s, as projected by current models,[85−87] underscore the significance of our FYI Hg model. This model is well-suited to investigate the potential alterations in polar Hg cycling in response to climate change. Our findings can inform assessments of Hg exposure to Arctic populations required by the effectiveness evaluation of the Minamata Convention on Mercury, facilitating the development of effective mitigation strategies.

■ ASSOCIATED CONTENT

Supporting Information

The Supporting Information is available free of charge at https://pubs.acs.org/doi/10.1021/acs.est.3c05080.

Sea ice area variation: Annual and monthly variation of sea ice area in the Arctic Ocean and the Southern Ocean; sea ice concentration distribution: Seasonal distribution of sea ice concentrations in the Arctic Ocean and the Southern Ocean; Arctic sea ice age simulation: simulated age of Arctic sea ice in September 2010; sensitivity analysis of snow Hg concentrations: sensitivity analysis of snow Hg concentrations under four deposition schemes; sea ice Hg^0 re-emission sensitivity: sensitivity analysis of

https://doi.org/10.1021/acs.est.3c05080
Environ. Sci. Technol. XXXX, XXX, XXX−XXX

various Hg^0 re-emission fractions; deposition flux of Hg: seasonal deposition fluxes of Hg to the snow cover above sea ice in polar oceans; Hg^0 re-emission flux from snow cover: seasonal fluxes of Hg^0 re-emission from snow cover in the polar oceans; Hg fluxes in sea ice: seasonal Hg fluxes of various processes to the sea ice environment in the polar oceans; and observation data: detailed information of observation data used for model validation (PDF)

AUTHOR INFORMATION

Corresponding Author

Yanxu Zhang − *School of Atmospheric Sciences, Nanjing University, Nanjing 210023, China; Frontiers Science Center for Critical Earth Material Cycling, Nanjing University, Nanjing 210023 Jiangsu, China;* orcid.org/0000-0001-7770-3466; Email: zhangyx@nju.edu.cn

Authors

Shaojian Huang − *School of Atmospheric Sciences, Nanjing University, Nanjing 210023, China*

Feiyue Wang − *Centre for Earth Observation Science, and Department of Environment and Geography, University of Manitoba, Winnipeg MB R3T 2N2, Canada;* orcid.org/0000-0001-5297-0859

Tengfei Yuan − *School of Atmospheric Sciences, Nanjing University, Nanjing 210023, China*

Zhengcheng Song − *School of Atmospheric Sciences, Nanjing University, Nanjing 210023, China*

Peipei Wu − *School of Atmospheric Sciences, Nanjing University, Nanjing 210023, China*

Complete contact information is available at: https://pubs.acs.org/10.1021/acs.est.3c05080

Notes

The authors declare no competing financial interest.

ACKNOWLEDGMENTS

The authors gratefully acknowledge the financial support from the National Natural Science Foundation of China (NNSFC) (42177349), the Fundamental Research Funds for the Central Universities (14380188 and 14380168), Frontiers Science Center for Critical Earth Material Cycling, the Collaborative Innovation Center of Climate Change, Jiangsu Province, and the Canada Research Chairs Program (F.W.).

REFERENCES

(1) AMAP. AMAP Assessment 2021: Mercury in the Arctic. *Arctic Monitoring and Assessment Programme (AMAP)*: Tromsø, Norway, 2021;. vii + 230pp.

(2) Beattie, S. A.; Armstrong, D.; Chaulk, A.; Comte, J.; Gosselin, M.; Wang, F. Total and Methylated Mercury in Arctic Multiyear Sea Ice. *Environ. Sci. Technol.* **2014**, *48*, 5575−5582.

(3) Dastoor, A.; Angot, H.; Bieser, J.; Christensen, J. H.; Douglas, T. A.; Heimbürger-Boavida, L. E.; Jiskra, M.; Mason, R. P.; McLagan, D. S.; Obrist, D.; Outridge, P. M.; Petrova, M. V.; Ryjkov, A.; St Pierre, K. A.; Schartup, A. T.; Soerensen, A. L.; Toyota, K.; Travnikov, O.; Wilson, S. J.; Zdanowicz, C. Arctic Mercury Cycling. *Nat. Rev. Earth Environ.* **2022**, *3*, 270−286.

(4) Schartup, A. T.; Soerensen, A. L.; Heimbürger-Boavida, L.-E. Influence of the Arctic Sea-Ice Regime Shift on Sea-Ice Methylated Mercury Trends. *Environ. Sci. Technol. Lett.* **2020**, *7*, 708−713.

(5) Lalonde, J. D.; Poulain, A. J.; Amyot, M. The Role of Mercury Redox Reactions in Snow on Snow-to-Air Mercury Transfer. *Environ. Sci. Technol.* **2002**, *36*, 174−178.

(6) Lindberg, S. E.; Brooks, S.; Lin, C. J.; Scott, K. J.; Landis, M. S.; Stevens, R. K.; Goodsite, M.; Richter, A. Dynamic Oxidation of Gaseous Mercury in the Arctic Troposphere at Polar Sunrise. *Environ. Sci. Technol.* **2002**, *36*, 1245−1256.

(7) Soerensen, A. L.; Jacob, D. J.; Schartup, A. T.; Fisher, J. A.; Lehnherr, I.; St Louis, V. L.; Heimbürger, L. E.; Sonke, J. E.; Krabbenhoft, D. P.; Sunderland, E. M. A Mass Budget for Mercury and Methylmercury in the Arctic Ocean. *Global Biogeochem. Cycles* **2016**, *30*, 560−575.

(8) Wang, K.; Munson, K. M.; Beaupré-Laperrière, A.; Mucci, A.; Macdonald, R. W.; Wang, F. Subsurface Seawater Methylmercury Maximum Explains Biotic Mercury Concentrations in the Canadian Arctic. *Sci. Rep.* **2018**, *8*, 14465.

(9) United Nations Environment Programme (UNEP). Minamata Convention on Mercury. http://www.mercuryconvention.org (accessed Nov 24, 2020).

(10) Kort, E. A.; Wofsy, S. C.; Daube, B. C.; Diao, M.; Elkins, J. W.; Gao, R. S.; Hintsa, E. J.; Hurst, D. F.; Jimenez, R.; Moore, F. L.; Spackman, J. R.; Zondlo, M. A. Atmospheric Observations of Arctic Ocean Methane Emissions up to 82° North. *Nat. Geosci.* **2012**, *5*, 318−321.

(11) Wang, F.; Pućko, M.; Stern, G. Transport and Transformation of Contaminants in Sea Ice. *Sea Ice*, 3rd ed.; Wiley-Blackwell, 2017; pp. 472−491. DOI: DOI: 10.1002/9781118778371.ch19.

(12) Thomas, D. N.; Papadimitriou, S.; Michel, C. Biogeochemistry of Sea Ice. In *Sea Ice*, 2nd ed.; Thomas, D. N.; Dieckmann, G. S., Eds.; Wiley-Blackwell: Chichester, U.K., 2010; pp. 425−467.

(13) Nerentorp Mastromonaco, M. G.; Gårdfeldt, K.; Langer, S.; Dommergue, A. Seasonal Study of Mercury Species in the Antarctic Sea Ice Environment. *Environ. Sci. Technol.* **2016**, *50*, 12705−12712.

(14) Nghiem, S. V.; Rigor, I. G.; Perovich, D. K.; Clemente-Colon, P.; Weatherly, J. W.; Neumann, G. Rapid Reduction of Arctic Perennial Sea Ice. *Geophys. Res. Lett.* **2007**, *34*, L19504.

(15) Chaulk, A.; Stern, G. A.; Armstrong, D.; Barber, D. G.; Wang, F. Mercury Distribution and Transport across the Ocean-Sea-Ice-Atmosphere Interface in the Arctic Ocean. *Environ. Sci. Technol.* **2011**, *45*, 1866−1872.

(16) Zheng, W.; Chandan, P.; Steffen, A.; Stupple, G.; De Vera, J.; Mitchell, C. P. J.; Wania, F.; Bergquist, B. A. Mercury Stable Isotopes Reveal the Sources and Transformations of Atmospheric Hg in the High Arctic. *Appl. Geochem.* **2021**, *131*, 105002.

(17) Durnford, D.; Dastoor, A. The Behavior of Mercury in the Cryosphere: A Review of What We Know from Observations. *J. Geophys. Res.: Atmos.* **2011**, *116*, D06305.

(18) Albert, M. R.; Shultz, E. F. Snow and Firn Properties and Air-Snow Transport Processes at Summit, Greenland. *Atmos. Environ.* **2002**, *36*, 2789−2797.

(19) Anderson, P. S.; Neff, W. D. Boundary Layer Physics over Snow and Ice. *Atmos. Chem. Phys.* **2008**, *8*, 3563−3582.

(20) Kuhn, M. The Nutrient Cycle through Snow and Ice, a Review. *Aquat. Sci.* **2001**, *63*, 150−167.

(21) Cox, G. F. N.; Weeks, W. F. Salinity Variations in Sea Ice. *J. Glaciol.* **1974**, *13*, 109−120.

(22) Cox, G. F. N.; Weeks, W. F. Numerical Simulations of the Profile Properties of Undeformed First-Year Sea Ice during the Growth Season. *J. Geophys. Res.* **1988**, *93*, 12449−12460.

(23) DiMento, B. P.; Mason, R. P.; Brooks, S.; Moore, C. The Impact of Sea Ice on the Air-Sea Exchange of Mercury in the Arctic Ocean. *Deep Sea Res., Part I* **2019**, *144*, 28−38.

(24) Brooks, S.; Lindberg, S.; Southworth, G.; Arimoto, R. Springtime Atmospheric Mercury Speciation in the McMurdo, Antarctica Coastal Region. *Atmos. Environ.* **2008**, *42*, 2885−2893.

(25) Dommergue, A.; Sprovieri, F.; Pirrone, N.; Ebinghaus, R.; Brooks, S.; Courteaud, J.; Ferrari, C. P. Overview of Mercury Measurements in the Antarctic Troposphere. *Atmos. Chem. Phys.* **2010**, *10*, 3309−3319.

(26) Johnson, K. P.; Blum, J. D.; Keeler, G. J.; Douglas, T. A. Investigation of the deposition and emission of mercury in arctic snow

during an atmospheric mercury depletion event. *J. Geophys. Res.: Atmos.* **2008**, *113*, D17304.
(27) St. Louis, V. L.; Sharp, M. J.; Steffen, A.; May, A.; Barker, J.; Kirk, J. L.; Kelly, D. J. A.; Arnott, S. E.; Keatley, B.; Smol, J. P. Some Sources and Sinks of Monomethyl and Inorganic Mercury on Ellesmere Island in the Canadian High Arctic. *Environ. Sci. Technol.* **2005**, *39*, 2686−2701.
(28) Araujo, B. F.; Osterwalder, S.; Szponar, N.; Lee, D.; Petrova, M. V.; Pernov, J. B.; Ahmed, S.; Heimbürger-Boavida, L.-E.; Laffont, L.; Teisserenc, R.; Tananaev, N.; Nordstrom, C.; Magand, O.; Stupple, G.; Skov, H.; Steffen, A.; Bergquist, B.; Pfaffhuber, K. A.; Thomas, J. L.; Scheper, S.; Petäjä, T.; Dommergue, A.; Sonke, J. E. Mercury Isotope Evidence for Arctic Summertime Re-Emission of Mercury from the Cryosphere. *Nat. Commun.* **2022**, *13*, 4956.
(29) Jiskra, M.; Sonke, J. E.; Agnan, Y.; Helmig, D.; Obrist, D. Insights from Mercury Stable Isotopes on Terrestrial-Atmosphere Exchange of Hg(0) in the Arctic Tundra. *Biogeosciences* **2019**, *16*, 4051−4064.
(30) Mann, E. A.; Mallory, M. L.; Ziegler, S. E.; Tordon, R.; O'Driscoll, N. J. Mercury in Arctic Snow: Quantifying the Kinetics of Photochemical Oxidation and Reduction. *Sci. Total Environ.* **2015**, *509*−*510*, 115−132.
(31) Mann, E. A.; Ziegler, S. E.; Steffen, A.; O'Driscoll, N. J. Increasing Chloride Concentration Causes Retention of Mercury in Melted Arctic Snow Due to Changes in Photoreduction Kinetics. *J. Environ. Sci.* **2018**, *68*, 122−129.
(32) Štrok, M.; Baya, P. A.; Hintelmann, H. The Mercury Isotope Composition of Arctic Coastal Seawater. *Compt. Rendus Geosci.* **2015**, *347*, 368−376.
(33) Fisher, J. A.; Jacob, D. J.; Soerensen, A. L.; Amos, H. M.; Corbitt, E. S.; Streets, D. G.; Wang, Q.; Yantosca, R. M.; Sunderland, E. M. Factors Driving Mercury Variability in the Arctic Atmosphere and Ocean over the Past 30 Years. *Global Biogeochem. Cycles* **2013**, *27*, 1226−1235.
(34) Fisher, J. A.; Jacob, D. J.; Soerensen, A. L.; Amos, H. M.; Steffen, A.; Sunderland, E. M. Riverine Source of Arctic Ocean Mercury Inferred from Atmospheric Observations. *Nat. Geosci.* **2012**, *5*, 499−504.
(35) Song, S.; Angot, H.; Selin, N.; Gallée, H.; Sprovieri, F.; Pirrone, N.; Helmig, D.; Savarino, J.; Magand, O.; Dommergue, A. Understanding Mercury Oxidation and Air-Snow Exchange on the East Antarctic Plateau: A Modeling Study. *Atmos. Chem. Phys.* **2018**, *18*, 15825−15840.
(36) Losch, M.; Menemenlis, D.; Campin, J. M.; Heimbach, P.; Hill, C. On the Formulation of Sea-Ice Models. Part 1: Effects of Different Solver Implementations and Parameterizations. *Ocean Model.* **2010**, *33*, 129−144.
(37) Zhang, Y.; Jacob, D. J.; Dutkiewicz, S.; Amos, H. M.; Long, M. S.; Sunderland, E. M. Biogeochemical Drivers of the Fate of Riverine Mercury Discharged to the Global and Arctic Oceans. *Global Biogeochem. Cycles* **2015**, *29*, 854−864.
(38) Zhang, Y.; Soerensen, A. L.; Schartup, A. T.; Sunderland, E. M. A Global Model for Methylmercury Formation and Uptake at the Base of Marine Food Webs. *Global Biogeochem. Cycles* **2020**, *34*, No. e2019GB006348.
(39) Forget, G.; Campin, J.-M.; Heimbach, P.; Hill, C. N.; Ponte, R. M.; Wunsch, C. ECCO Version 4: An Integrated Framework for Non-Linear Inverse Modeling and Global Ocean State Estimation. *Geosci. Model Dev.* **2015**, *8*, 3071−3104.
(40) Hibler, W. D. A Dynamic Thermodynamic Sea Ice Model. *J. Phys. Oceanogr.* **1979**, *9*, 815−846.
(41) Hibler, W. D. Modeling a Variable Thickness Sea Ice Cover. *Mon. Weather Rev.* **1980**, *108*, 1943−1973.
(42) Zhang, J.; Hibler, W. D. On an Efficient Numerical Method for Modeling Sea Ice Dynamics. *J. Geophys. Res.: Oceans* **1997**, *102*, 8691−8702.
(43) Zheng, F.; Sun, Y.; Yang, Q.; Mu, L. Evaluation of Arctic Sea-Ice Cover and Thickness Simulated by MITgcm. *Adv. Atmos. Sci.* **2021**, *38*, 29−48.
(44) Rigor, I. G.; Wallace, J. M. Variations in the Age of Arctic Sea-Ice and Summer Sea-Ice Extent. *Geophys. Res. Lett.* **2004**, *31*, L09401.
(45) Zhang, J.; Rothrock, D. A.; Steele, M. Warming of the Arctic Ocean by a Strengthened Atlantic Inflow: Model Results. *Geophys. Res. Lett.* **1998**, *25*, 1745−1748.
(46) Lepparanta, M. A Growth Model for Black Ice, Snow Ice and Snow Thickness in Subarctic Basins. *Nord. Hydrol* **1983**, *14*, 59−70.
(47) Douglas, T. A.; Sturm, M.; Simpson, W. R.; Blum, J. D.; Alvarez-Aviles, L.; Keeler, G. J.; Perovich, D. K.; Biswas, A.; Johnson, K. Influence of Snow and Ice Crystal Formation and Accumulation on Mercury Deposition to the Arctic. *Environ. Sci. Technol.* **2008**, *42*, 1542−1551.
(48) Steffen, A.; Douglas, T.; Amyot, M.; Ariya, P.; Aspmo, K.; Berg, T.; Bottenheim, J.; Brooks, S.; Cobbett, F.; Dastoor, A.; Dommergue, A.; Ebinghaus, R.; Ferrari, C.; Gardfeldt, K.; Goodsite, M. E.; Lean, D.; Poulain, A. J.; Scherz, C.; Skov, H.; Sommar, J.; Temme, C. A Synthesis of Atmospheric Mercury Depletion Event Chemistry in the Atmosphere and Snow. *Atmos. Chem. Phys.* **2008**, *8*, 1445−1482.
(49) Horowitz, H. M.; Jacob, D. J.; Zhang, Y.; DIbble, T. S.; Slemr, F.; Amos, H. M.; Schmidt, J. A.; Corbitt, E. S.; Marais, E. A.; Sunderland, E. M. A New Mechanism for Atmospheric Mercury Redox Chemistry: Implications for the Global Mercury Budget. *Atmos. Chem. Phys.* **2017**, *17*, 6353−6371.
(50) Zhang, Y.; Jacob, D. J.; Horowitz, H. M.; Chen, L.; Amos, H. M.; Krabbenhoft, D. P.; Slemr, F.; St Louis, V. L.; Sunderland, E. M. Observed Decrease in Atmospheric Mercury Explained by Global Decline in Anthropogenic Emissions. *Proc. Natl. Acad. Sci. U.S.A.* **2016**, *113*, 526−531.
(51) Song, Z.; Sun, R.; Zhang, Y. Modeling Mercury Isotopic Fractionation in the Atmosphere. *Environ. Pollut.* **2022**, *307*, 119588.
(52) Shah, V.; Jacob, D. J.; Thackray, C. P.; Wang, X.; Sunderland, E. M.; Dibble, T. S.; Saiz-Lopez, A.; Černušák, I.; Kellö, V.; Castro, P. J.; Wu, R.; Wang, C. Improved Mechanistic Model of the Atmospheric Redox Chemistry of Mercury. *Environ. Sci. Technol.* **2021**, *55*, 14445−14456.
(53) Overland, J. E.; Wang, M. Y. When Will the Summer Arctic Be Nearly Sea Ice Free? *Geophys. Res. Lett.* **2013**, *40*, 2097−2101.
(54) Wang, M. Y.; Overland, J. E. A Sea Ice Free Summer Arctic within 30 Years? *Geophys. Res. Lett.* **2009**, *36*, L07502.
(55) Ferrari, C. P.; Gauchard, P. A.; Aspmo, K.; Dommergue, A.; Magand, O.; Bahlmann, E.; Nagorski, S.; Temme, C.; Ebinghaus, R.; Steffen, A.; Banic, C.; Berg, T.; Planchon, F.; Barbante, C.; Cescon, P.; Boutron, C. F. Snow-to-air exchanges of mercury in an Arctic seasonal snow pack in Ny-Ålesund, Svalbard. *Atmos. Environ.* **2005**, *39*, 7633−7645.
(56) Durnford, D.; Dastoor, A.; Ryzhkov, A.; Poissant, L.; Pilote, M.; Figueras-Nieto, D. How Relevant Is the Deposition of Mercury onto Snowpacks?-Part 2: A Modeling Study. *Atmos. Chem. Phys.* **2012**, *12*, 9251−9274.
(57) Weeks, W. F.; Ackley, S. F. The Growth, Structure, and Properties of Sea Ice. In *The Geophysics of Sea Ice*; Untersteiner, N., Ed.; *NATO ASI Series*; Springer: Boston, MA, 1986; pp 9−164. DOI: DOI: 10.1007/978-1-4899-5352-0_2.
(58) Vancoppenolle, M.; Bitz, C. M.; Fichefet, T. Summer Landfast Sea Ice Desalination at Point Barrow, Alaska: Modeling and Observations. *J. Geophys. Res.: Oceans* **2007**, *112*, C04022.
(59) Ebinghaus, R.; Jennings, S. G.; Schroeder, W. H.; Berg, T.; Donaghy, T.; Guentzel, J.; Kenny, C.; Kock, H. H.; Kvietkus, K.; Landing, W.; Mühleck, T.; Munthe, J.; Prestbo, E. M.; Schneeberger, D.; Slemr, F.; Sommar, J.; Urba, A.; Wallschläger, D.; Xiao, Z. International Field Intercomparison Measurements of Atmospheric Mercury Species at Mace Head, Ireland. *Atmos. Environ.* **1999**, *33*, 3063−3073.
(60) Gårdfeldt, K.; Sommar, J.; Strömberg, D.; Feng, X. Oxidation of Atomic Mercury by Hydroxyl Radicals and Photoinduced Decomposition of Methylmercury in the Aqueous Phase. *Atmos. Environ.* **2001**, *35*, 3039−3047.

https://doi.org/10.1021/acs.est.3c05080
Environ. Sci. Technol. XXXX, XXX, XXX−XXX

(61) Sturm, M.; Massom, R. A. Snow in the Sea Ice System: Friend or Foe? In *Sea Ice*, 3rd ed.; Wiley-Blackwell, 2016; pp. 65−109. DOI: DOI: 10.1002/9781118778371.ch3.
(62) Steffen, A.; Bottenheim, J.; Cole, A.; Douglas, T. A.; Ebinghaus, R.; Friess, U.; Netcheva, S.; Nghiem, S.; Sihler, H.; Staebler, R. Atmospheric Mercury over Sea Ice during the OASIS-2009 Campaign. *Atmos. Chem. Phys.* **2013**, *13*, 7007−7021.
(63) Faïn, X.; Ferrari, C. P.; Dommergue, A.; Albert, M.; Battle, M.; Arnaud, L.; Barnola, J. M.; Cairns, W.; Barbante, C.; Boutron, C. Mercury in the Snow and Firn at Summit Station, Central Greenland, and Implications for the Study of Past Atmospheric Mercury Levels. *Atmos. Chem. Phys.* **2008**, *8*, 3441−3457.
(64) Massman, W. J. Molecular Diffusivities of Hg Vapor in Air, O2 and N2 near STP and the Kinematic Viscosity and Thermal Diffusivity of Air near STP. *Atmos. Environ.* **1999**, *33*, 453−457.
(65) Soerensen, A. L.; Sunderland, E. M.; Holmes, C. D.; Jacob, D. J.; Yantosca, R. M.; Skov, H.; Christensen, J. H.; Strode, S. A.; Mason, R. P. An Improved Global Model for Air-Sea Exchange of Mercury: High Concentrations over the North Atlantic. *Environ. Sci. Technol.* **2010**, *44*, 8574−8580.
(66) Manizza, M.; Follows, M. J.; Dutkiewicz, S.; McClelland, J. W.; Menemenlis, D.; Hill, C. N.; Townsend-Small, A.; Peterson, B. J. Modeling Transport and Fate of Riverine Dissolved Organic Carbon in the Arctic Ocean. *Global Biogeochem. Cycles* **2009**, *23*, GB4006.
(67) Dee, D. P.; Uppala, S. M.; Simmons, A. J.; Berrisford, P.; Poli, P.; Kobayashi, S.; Andrae, U.; Balmaseda, M. A.; Balsamo, G.; Bauer, P.; Bechtold, P.; Beljaars, A. C. M.; van de Berg, L.; Bidlot, J.; Bormann, N.; Delsol, C.; Dragani, R.; Fuentes, M.; Geer, A. J.; Haimberger, L.; Healy, S. B.; Hersbach, H.; Hólm, E. V.; Isaksen, L.; Kållberg, P.; Köhler, M.; Matricardi, M.; McNally, A. P.; Monge-Sanz, B. M.; Morcrette, J.-J.; Park, B.-K.; Peubey, C.; de Rosnay, P.; Tavolato, C.; Thépaut, J.-N.; Vitart, F. The ERA-Interim Reanalysis: Configuration and Performance of the Data Assimilation System. *Q. J. R. Meteorol. Soc.* **2011**, *137*, 553−597.
(68) Liu, M.; Zhang, Q.; Maavara, T.; Liu, S.; Wang, X.; Raymond, P. A. Rivers as the Largest Source of Mercury to Coastal Oceans Worldwide. *Nat. Geosci.* **2021**, *14*, 672−677.
(69) Xu, L.; Russell, L. M.; Somerville, R. C. J.; Quinn, P. K. Frost Flower Aerosol Effects on Arctic Wintertime Longwave Cloud Radiative Forcing. *J. Geophys. Res.: Atmos.* **2013**, *118*, 13282−13291.
(70) Nussbaumer, E. A.; Pinker, R. T. The Role of Shortwave Radiation in the 2007 Arctic Sea Ice Anomaly. *Geophys. Res. Lett.* **2012**, *39*, L15808.
(71) Lu, J. Y.; Schroeder, W. H.; Barrie, L. A.; Steffen, A.; Welch, H. E.; Martin, K.; Lockhart, L.; Hunt, R. V.; Boila, G.; Richter, A. Magnification of Atmospheric Mercury Deposition to Polar Regions in Springtime: The Link to Tropospheric Ozone Depletion Chemistry. *Geophys. Res. Lett.* **2001**, *28*, 3219−3222.
(72) Aspmo, K.; Temme, C.; Berg, T.; Ferrari, C.; Gauchard, P.-A.; Fain, X.; Wibetoe, G. Mercury in the Atmosphere, Snow and Melt Water Ponds in the North Atlantic Ocean during Arctic Summer. *Environ. Sci. Technol.* **2006**, *40*, 4083−4089.
(73) Serreze, M. C.; Meier, W. N. The Arctic's Sea Ice Cover: Trends, Variability, Predictability, and Comparisons to the Antarctic. *Ann. N.Y. Acad. Sci.* **2019**, *1436*, 36−53.
(74) Nicolaus, M.; Haas, C.; Willmes, S. Evolution of First-Year and Second-Year Snow Properties on Sea Ice in the Weddell Sea during Spring-Summer Transition. *J. Geophys. Res.: Atmos.* **2009**, *114*, D17109.
(75) Kirk, J. L.; St Louis, V. L.; Sharp, M. J. Rapid Reduction and Reemission of Mercury Deposited into Snowpacks during Atmospheric Mercury Depletion Events at Churchill, Manitoba, Canada. *Environ. Sci. Technol.* **2006**, *40*, 7590−7596.
(76) Jeffries, M. O.; Adolphs, U. Early Winter Ice and Snow Thickness Distribution, Ice Structure and Development of the Western Ross Sea Pack Ice between the Ice Edge and the Ross Ice Shelf. *Antarct. Sci.* **1997**, *9*, 188−200.
(77) Massom, R. A.; Eicken, H.; Hass, C.; Jeffries, M. O.; Drinkwater, M. R.; Sturm, M.; Worby, A. P.; Wu, X.; Lytle, V. I.; Ushio, S.; Morris, K.; Reid, P. A.; Warren, S. G.; Allison, I. Snow on Antarctic Sea Ice. *Rev. Geophys.* **2001**, *39*, 413−445.
(78) Sturm, M.; Morris, K.; Massom, R. *The Winter Snow Cover of the West Antarctic Pack Ice: Its Spatial and Temporal Variability*; American Geophysical Union, 1998; Vol. *74*, pp 1−18. DOI: DOI: 10.1029/ar074p0001.
(79) Warren, S. G.; Rigor, I. G.; Untersteiner, N.; Radionov, V. F.; Bryazgin, N. N.; Aleksandrov, Y. I.; Colony, R. Snow Depth on Arctic Sea Ice. *J. Clim.* **1999**, *12*, 1814−1829.
(80) Wettlaufer, J. S.; Worster, M. G.; Huppert, H. E. The Phase Evolution of Young Sea Ice. *Geophys. Res. Lett.* **1997**, *24*, 1251−1254.
(81) Petrich, C.; Eicken, H. Overview of Sea Ice Growth and Properties. *Sea Ice*, 3rd ed.; Wiley-Blackwell, 2016; pp. 1−41. DOI: DOI: 10.1002/9781118778371.ch1.
(82) Dethleff, D.; Kuhlmann, G. Entrainment of Fine-Grained Surface Deposits into New Ice in the Southwestern Kara Sea, Siberian Arctic. *Cont. Shelf Res.* **2009**, *29*, 691−701.
(83) Reimnitz, E.; Barnes, P. W.; Weber, W. S. Particulate matter in pack ice of the Beaufort Gyre. *J. Glaciol.* **1993**, *39*, 186−198.
(84) Sonke, J. E.; Teisserenc, R.; Heimbürger-Boavida, L. E.; Petrova, M. V.; Marusczak, N.; Le Dantec, T.; Chupakov, A. V.; Li, C.; Thackray, C. P.; Sunderland, E. M.; Tananaev, N.; Pokrovsky, O. S. Eurasian River Spring Flood Observations Support Net Arctic Ocean Mercury Export to the Atmosphere and Atlantic Ocean. *Proc. Natl. Acad. Sci. U.S.A.* **2018**, *115*, E11586−E11594.
(85) Bonan, D. B.; Schneider, T.; Eisenman, I.; Wills, R. C. J. Constraining the Date of a Seasonally Ice-Free Arctic Using a Simple Model. *Geophys. Res. Lett.* **2021**, *48*, No. e2021GL094309.
(86) Årthun, M.; Onarheim, I. H.; Dörr, J.; Eldevik, T. The Seasonal and Regional Transition to an Ice-Free Arctic. *Geophys. Res. Lett.* **2021**, *48*, No. e2020GL090825.
(87) Screen, J. A.; Blackport, R. How Robust Is the Atmospheric Response to Projected Arctic Sea Ice Loss Across Climate Models? *Geophys. Res. Lett.* **2019**, *46*, 11406−11415.

https://doi.org/10.1021/acs.est.3c05080
Environ. Sci. Technol. XXXX, XXX, XXX−XXX